Systematics of α-decay half-lives around shell closures

M. Ismail, A. Y. Ellithi, M. M. Botros, and A. Adel*
Physics Department, Faculty of Science, Cairo University, Egypt
(Received 28 October 2009; revised manuscript received 10 January 2010; published 10 February 2010)

We present a systematic calculation of α-decay half-lives of even-even heavy and superheavy nuclei in the framework of the preformed α model. The microscopic α-daughter nuclear interaction potential is calculated by double-folding the density distributions of both α and daughter nuclei with a realistic effective Michigan three-Yukawa nucleon-nucleon interaction, and the microscopic Coulomb potential is calculated by folding the charge density distributions of the two interacting nuclei. The half-lives are found to be sensitive to the density dependence of the nucleon-nucleon interaction and the implementation of the Bohr-Sommerfeld quantization condition inherent in the Wentzel-Kramers-Brillouin approach. The α-decay half-lives obtained agree reasonably well with the available experimental data. Moreover, the study has been extended to the newly observed superheavy nuclei. The interplay of closed-shell effects in α-decay calculations is investigated. The α-decay calculations give the closed-shell effects of known spherical magicities, $Z = 82$ and $N = 126$, and further predict enhanced stabilities at $N = 152$, 162, and 184 for $Z = 100$, 108, and 114, owing to the stability of parent nuclei against α decays. It is worth noting that the aim of this work is not only to reproduce the experimental data better, but also to extend our understanding of α-decay half-lives around shell closures.

DOI: 10.1103/PhysRevC.81.024602 PACS number(s): 23.60.+e, 21.10.Tg, 27.80.+w, 27.90.+b

I. INTRODUCTION

One of the most important decay modes for unstable medium and heavy nuclei is α radioactivity [1,2]. In recent years, there has been renewed interest in α decay because of the development of radioactive beams and new low-temperature detector technology. Thanks to these new developments, α decay is now a powerful tool for investigating the details of nuclear structure [3], for example, α clustering, shell effect, effective nuclear interaction, and nuclear deformation. In recent experiments on superheavy nuclei, α decay has been used as a reliable way to identify new synthesized superheavy elements (SHEs) and isomeric states, which is a hot topic in nuclear physics [2,4].

From the theoretical side, the process of α decay is fundamentally a quantum-tunneling effect, which was explained independently by Gamow [5] and Condon and Gurney [6] in the 1920s. This was the first successful application of quantum mechanics to a nuclear physics problem and was rather groundbreaking in the development of nuclear physics. Subsequently, a number of theoretical calculations were performed by both phenomenological and microscopic methods to predict absolute α-decay width, to extract nuclear structure information, and to pursue a microscopic understanding of α-decay phenomenon. For instance, Buck *et al.* systematically calculated the α-decay half-lives of nuclei by using the Cosh potential [7]. The density-dependent Michigan three-Yukawa (M3Y) interaction and the mean-field potential have also been applied to the calculation of α-decay half-lives [8–18].

A semiclassical formulation of the problem of the penetration of an α particle through the barrier, based on the Wentzel-Kramers-Brillouin (WKB) approximation [19,20], was found to be a suitable approximation. The decay width in general was defined as a product of the frequency of collisions of the α particle with the barrier (the so-called assault frequency) and the penetration probability [21,22]. In the calculation of α-decay half-lives, one has to invoke another indispensable quantity, that is, the α-cluster preformation factor (also called the spectroscopic factor, as it is related to the nuclear structure information). It gives the probability of finding the α particle preformed in the parent nucleus [21]. This quantity can be obtained microscopically by evaluating the squared product of the overlaps between the single-particle states in the many-body state of the α particle and those in the many-body state of the parent. Tonozuka and Arima [23] calculated the probability of an α cluster within the framework of the shell model. Horiuchi and Takemoto *et al.* [24,25] studied α-clustering structures in nuclei and in nuclear matter. Although many attempts have been made, the development of a theoretical description of the α-cluster preformation factor is slow, owing to the complexity of both the nuclear potential and the nuclear many-body problem.

In the present work, the half-lives of new SHEs have been determined using microscopic potentials within the semiclassical WKB approximation in combination with the Bohr-Sommerfeld quantization condition and compared with the existing theoretical and experimental results to test the extent of the validity of this formalism and its ability to predict magic numbers in the superheavy region. The nuclear potentials have been obtained by the double-folding of the α- and daughter-nucleus density distributions with free or density-dependent effective nucleon-nucleon (NN) interactions. The nuclear potential energy for the α-nucleus interaction has therefore been obtained microscopically.A double-folding potential obtained with the M3Y [26,27] effective interaction supplemented with a zero-range potential for single-nucleon exchange is more appropriate because of its microscopic nature [28]. The semirealistic explicit density

*ahmedshosha200@yahoo.com

dependence [29] in the M3Y effective interaction has also been employed to incorporate higher-order exchange and Pauli blocking effects.

The outline of the paper is as follows. In the next section, we present the formulas and parameters for effective NN interaction used in our calculations. In Sec. III, we describe the microscopic nuclear and Coulomb potentials between α and daughter nuclei. The extraction of the α-decay half-life from the microscopic calculations using the folding potential and the WKB approximation, with implementation of the Bohr-Sommerfeld quantization condition, is presented in Sec. IV. The calculated results are discussed in Sec.V. Finally, Sec. VI gives a brief conclusion.

II. EFFECTIVE NUCLEON-NUCLEON INTERACTION

The double-folding model for calculation of the nucleus-nucleus potential uses the two frozen densities $\rho_1(\vec{r}_1)$ and $\rho_2(\vec{r}_2)$, folded with a properly chosen effective NN interaction, υ_{NN}. The folding model can be considered to be a semimicroscopic approach, because no free parameters, except for an overall normalization, enter the calculation [27,30]. Once we have realistic nuclear densities, available from different nuclear models or directly from the electron scattering data, it still remains necessary to have a realistic effective NN interaction before the success of the folding model can be reliability assessed.

A variety of effective NN interactions has been introduced into the folding model, but the one that became known as M3Y is probably the most widely used and certainly is representative of "realistic interactions." Explicit forms for M3Y, effective, interactions are defined by [31]

$$\upsilon_{NN}(E,r) = \upsilon_{00}(r) + \hat{j}_{00}(E)\delta(r). \tag{1}$$

For M3Y, Reid form,

$$\upsilon_{00}(r) = \left[7999\,\frac{\exp(-4r)}{4r} - 2134\,\frac{\exp(-2.5r)}{2.5r}\right]\ \text{MeV}, \tag{2}$$

For M3Y, Paris form,

$$\upsilon_{00}(r) = \left[11062\,\frac{\exp(-4r)}{4r} - 2538\,\frac{\exp(-2.5r)}{2.5r}\right]\ \text{MeV}, \tag{3}$$

where the first term in Eq. (1) is the central NN force, and the second term is the zero-range pseudopotential term that represents the effects of single-nucleon knock-on exchange. The magnitude of $\hat{j}_{00}(E)$ for an M3Y—Reid interaction can be expressed as

$$\hat{j}_{00}(E) \approx -276\ [1 - 0.005\,(E/A)]\ \text{MeV fm}^3, \tag{4}$$

while use of the MY3—Paris form gives

$$\hat{j}_{00}(E) \approx -590\ [1 - 0.002\,(E/A)]\ \text{MeV fm}^3, \tag{5}$$

where E/A is the bombarding energy per projectile nucleon (MeV).

The effective interaction between two nucleons in a nucleus depends on the density of the surrounding medium [31,32]. The density-dependent M3Y interaction may be written in the form

$$\upsilon^{DD}(\rho,r) = f(\rho)\ \upsilon_{NN}(r), \tag{6}$$

where $\upsilon_{NN}(r)$ is the original M3Y interaction (including the knock-on pseudopotential). The first version [29,33] took $\upsilon_{NN}(r)$ to be an M3Y (Reid) interaction, Eq. (2), together with the knock-on exchange pseudopotential as in Eq. (4). The density dependence adopted [33] was

$$f(\rho) = C[1 + \alpha \exp(-\beta\rho)], \tag{7}$$

where parameters C, α, and β may depend on energy. The parameter values for the energy range $E = 3$ to 90 MeV per nucleon adopted for the density and energy dependence for Eq. (7) are given in Ref. [34].

One of the possible prescriptions for the density entering Eq. (7) is that ρ is the density midway between the two interacting nucleons, but in view of the short range of the effective interaction it is sufficiently accurate to use the more convenient form,

$$\rho = \rho_\alpha(\vec{r}_1) + \rho_d(\vec{r}_2), \tag{8}$$

where ρ_α and ρ_d are the densities of the α particle and the daughter nucleus, respectively. This choice allows for easy factorization of the density-dependent interaction necessary to perform the folding calculation in momentum space.

A reasonably good description of elastic α-nucleus scattering data was obtained by assuming another factorized form of this density dependence as follows:

$$f(\rho_\alpha, \rho_d) = C\left[1 - \beta\rho_\alpha^{2/3}\right]\left[1 - \beta\rho_d^{2/3}\right]. \tag{9}$$

Because the released energies involved in the cluster decay processes are very low compared to the energies in high-energy heavy-ion scattering, C and β were found to be energy independent and, for the case of the α decay of superheavy nuclei, C was chosen to be unity and $\beta = 1.6$ fm^2 [35,36]. This form of the density dependence has been used frequently in the α-nucleus potential for calculating α-decay half-lives [35,36].

III. THE α-NUCLEUS POTENTIAL

In the framework of the cluster model, the ground state of the parent nucleus is assumed to be an α cluster orbiting the daughter nucleus. The α-core potential is the sum of the nuclear potential, the Coulomb potential, and the centrifugal potential.

$$V(R) = V_N(R) + V_C(R) + \frac{\hbar^2(\ell + 1/2)^2}{2\mu\ R^2}, \tag{10}$$

where R is the separation distance between the center of mass of the α particle and that of the daughter nucleus. The latter term represents the Langer modified centrifugal barrier [37]. With the WKB approximation being valid for one-dimensional problems, the preceding modification from $\ell(\ell+1) \to (\ell + 1/2)^2$ is essential to ensure the correct behavior of the WKB scattered radial wave function near the origin [38]. ℓ is

the angular momentum of the α particle. μ is the reduced mass of the α-daughter system and is given by

$$\mu = \frac{M_e M_d}{M_e + M_d}, \tag{11}$$

where M_e and M_d are the masses of the emitted α particle and the daughter nucleus, respectively, all measured in units of MeV/c^2.

The nuclear potential $V_N(R)$ is obtained from the double-folding integral of the renormalized M3Y NN potential with the matter density distributions of the α-particle and daughter nucleus [27–33].

$$V_N(R) = \lambda \int d\vec{r}_1 \int d\vec{r}_2 \; \rho_\alpha(\vec{r}_1) \; \rho_d(\vec{r}_2) \; \upsilon_{NN}(|\vec{s}|), \tag{12}$$

where λ is the renormalization factor. ρ_α and ρ_d are the matter density distributions of the α-particle and daughter nucleus, respectively. The quantity $|\vec{s}|$ is the distance between a nucleon in the daughter and a nucleon in the α particle ($\vec{s} = \vec{R} + \vec{r}_2 - \vec{r}_1$). The matter density distribution of the α particle is a standard Gaussian form, namely,

$$\rho_\alpha(r_1) = 0.4229 \; \exp\left(-0.7024 \, r_1^2\right), \tag{13}$$

whose volume integral is equal to the mass number of the α particle A_α (=4). The matter density distribution for the daughter nucleus can be described by the spherically symmetric Fermi function,

$$\rho_d(r_2) = \frac{\rho_0}{1 + \exp\left(\frac{r_2 - c}{a}\right)}, \tag{14}$$

where the value of ρ_0 has been fixed by integrating the matter density distribution equivalent to the mass number of the residual daughter nucleus A_d.

The half-density radius c and the diffuseness a are given by [8,9,39]

$$c = 1.07 A_d^{1/3} \text{ fm}, \quad a = 0.54 \text{ fm}. \tag{15}$$

The M3Y NN interaction [27,31] is given by two direct terms with different ranges, Eq. (2), and by an exchange term with a δ interaction, Eq. (4). This exchange term is introduced to the M3Y interaction to guarantee the antisymmetrization of identical particles in both the α-particle and the daughter nucleus.

For the spherical-spherical interacting pair, the double-folding potential in Eq. (12) can be evaluated easily in momentum space [27]. It is given by

$$\begin{aligned} V_N(R) &= 8\,\lambda \int_0^\infty dk \; k^2 \; j_0(kr) \; \tilde{\upsilon}_{NN}(k) \int_0^\infty dr_1 r_1^2 j_0(kr_1) \, \rho_\alpha(r_1) \\ &\quad \times \int_0^\infty dr_2 r_2^2 j_0(kr_2) \, \rho_d(r_2), \end{aligned} \tag{16}$$

where for the M3Y—Reid NN potential,

$$\tilde{\upsilon}_{NN}(k) = 4\pi \left[\frac{7999}{4(16 + k^2)} - \frac{2134}{2.5(6.25 + k^2)}\right] - 276(1 - 0.005 E_\alpha / A_\alpha), \tag{17a}$$

and for the M3Y—Paris NN interaction,

$$\tilde{\upsilon}_{NN}(k) = 4\pi \left[\frac{11\,062}{4(16 + k^2)} - \frac{2538}{2.5(6.25 + k^2)}\right] - 590(1 - 0.002 E_\alpha / A_\alpha). \tag{17b}$$

One could further improve the double-folding potential by taking into account the density dependence of the NN interaction. In this case, Eq. (12) may be rewritten in the form,

$$V_N(R) = \lambda \int d\vec{r}_1 \int d\vec{r}_2 \; \rho_\alpha(\vec{r}_1) \; \rho_d(\vec{r}_2) \times f[\rho_\alpha(r_1), \rho_d(r_2)] \upsilon_{NN}(|\vec{s}|), \tag{18}$$

where $f(\rho_\alpha, \rho_d)$ may be taken to be either an exponential dependence on density as in Eqs. (7) and (8) or a power-law density dependence as in Eq. (9). For the factorized form of the density dependence considered in the present work, Eq. (18) can be simplified to a form like Eq. (16). For the density dependence given by Eq. (9), Eq. (18) becomes the same as Eq. (16) after replacing ρ_i with $\rho_i(1 - \beta\rho_i^{2/3})$ with $i = \alpha$ or d and multiplying λ by the constant C.

The Coulomb potential is obtained using a similar double-folding procedure for a proton-proton Coulomb interaction with the matter densities of the α and the daughter replaced by their respective charge density distributions ρ'_α and ρ'_d. Thus the double-folding Coulomb potential can be written as

$$V_C(R) = \int d\vec{r}_1 \int d\vec{r}_2 \; \frac{e^2}{|\vec{R} + \vec{r}_2 - \vec{r}_1|} \; \rho'_\alpha(\vec{r}_1) \; \rho'_d(\vec{r}_2). \tag{19}$$

The charge distributions are taken to have a similar form as the matter distributions, except for the fact that they are normalized to the number of protons in the *alpha* and daughter.

IV. HALF-LIVES OF α RADIOACTIVITY

The half-life of a parent nucleus decaying by means of α emission is calculated using different approaches [7–9,17,22,35,36] to the tunneling problem in the framework of the WKB approximation. Two of these approaches are frequently used in calculating the α-decay half-lives. The first one [35,36] is a super asymmetric fission model, which often neglects the Bohr-Sommerfeld condition and the Langer modification, which are essential ingredients [22] of the WKB approximation. In this case the renormalization factor λ becomes a free parameter determined from the best fit of the experimental α-decay half-lives. The second approach [7–9], the density-dependent cluster model, which is adopted in the present work for our study of α-decay half-lives around shell closures, takes into account the Langer modification and the Bohr-Sommerfeld condition. A detailed comparison of the expressions for the decay widths obtained within the semiclassical WKB approximation using different approaches to the tunneling problem is performed in Ref. [22].

In the present approach, there are three classical turning points, denoted R_1, R_2, and R_3, in order of increasing distance from the origin. These turning points are obtained by numerical solutions of the equation $V(R) = Q$, where Q is the experimental α-decay energy. It should be noted

that the introduction of the Langer modification, namely, $\ell(\ell+1) \to (\ell+1/2)^2$, for the radial one-dimensional WKB problem introduces the inner turning point, R_1, near the origin even for the $\ell = 0$ case. This detail has been missed in some works [35,36,40,41].

The renormalization factor λ in the nuclear potential, Eqs. (12) and (18), is not an adjustable parameter but it is determined separately for each decay by applying the Bohr-Sommerfeld quantization condition [22],

$$\int_{R_1}^{R_2} dR\ K(R) = (2n+1)\,\frac{\pi}{2} = (G-\ell+1)\,\frac{\pi}{2}, \qquad (20)$$

where the wave number $K(R)$ is given by

$$K(R) = \sqrt{\frac{2\mu}{\hbar^2}|V(R)-Q|}. \qquad (21)$$

The number of nodes are expressed as $n = (G-\ell)/2$, where G is a global quantum number obtained from fits to data [8,9,42] and ℓ is the orbital angular momentum carried by the α particle. We perform calculations in the superheavy region with two possible fitted values of G, namely, 20 and 22. This system of equations, involving the turning points and the Bohr-Sommerfeld condition, is numerically solved by a few iterations to an acceptable level of accuracy.

Once the values of turning points together with the depth of the nuclear potential have been determined, we can calculate the α-decay width Γ of the quasibound state, in semiclassical approximation, by following the procedure of Gurvit and Kälbermann [43]. Using a one-dimensional WKB approximation, the barrier penetrability P is calculated within the action integral as

$$P = \exp\left[-2\int_{R_2}^{R_3} dR\ K(R)\right], \qquad (22)$$

In the quasiclassical approximation, the α-decay width Γ is [7,9,42]

$$\Gamma = P_\alpha\ F\ \frac{\hbar^2}{4\,\mu}\ \exp\left[-2\int_{R_2}^{R_3} dR\ K(R)\right], \qquad (23)$$

where P_α is the preformation probability of the α particle in a parent nucleus. It is very difficult to determine the preformation factor microscopically from current nuclear models owing to the complexity of the nuclear many-body problem. Experimentally the preformation factor does not change much for open-shell nuclei [44]. To simplify our calculations, we take the preformation factor as a constant for the same kind of nuclei and its value is chosen to give the best fit between experimental half-lives and theoretical ones [8,9]. This means that we have only a single adjustable parameter P_α for different kinds of nuclei. Here we choose the preformation probability $P_\alpha = 1.0$ for even-even superheavy nuclei. Moreover, a set of parameters of the preformation factors $P_\alpha = 0.38$ or 0.43, for even-even nuclei with $Z = 52$–105, has also been used, as in Refs. [8] and [9]. These values agree approximately with the experimental data for open-shell nuclei [44].

The normalization factor F is given by

$$F\int_{R_1}^{R_2} dR\ \frac{1}{K(R)}\cos^2\left[\int_{R_1}^{R} dR'\ K\left(R'\right) - \frac{\pi}{4}\right] = 1, \qquad (24)$$

where the squared cosine term may be replaced by $1/2$ without significant loss of accuracy [9,42,43]. This factor arises from the normalization of the bound-state wave function in the region between R_1 and R_2. Indeed, this factor is related to the so-called "assault frequency" of the tunneling particle at the barrier. The time interval Δt for the particle traversing a distance ΔR can be expressed as

$$\Delta t = \frac{\Delta R}{\nu(R)} = \frac{\mu\ \Delta R}{\hbar\ K(R)}. \qquad (25)$$

The assault frequency ν can be written as the inverse of the time required to traverse the distance back and forth between the turning points R_1 and R_2 as [22]

$$\nu = T^{-1} = \frac{\hbar}{2\mu}\left[\int_{R_1}^{R_2}\frac{dR}{K(R)}\right]^{-1}. \qquad (26)$$

In this way, we can write the α-decay width Γ in terms of the assault frequency ν as

$$\Gamma = P_\alpha\,\hbar\nu\ \exp\left[-2\int_{R_2}^{R_3} dR\ K(R)\right]. \qquad (27)$$

The α-decay half-life is then related to the width Γ by

$$T_{1/2} = \hbar\ln(2)/\Gamma. \qquad (28)$$

To extend the α-decay width to the deformed case, we assume that a spherical α particle interacts with an axially symmetric deformed daughter nucleus. The density distribution of the deformed daughter nucleus is given by

$$\rho_d\left(r_2,\ \theta\right) = \frac{\rho_0}{1+\exp\left[\frac{r_2-R(\theta)}{a}\right]}. \qquad (29)$$

The half-density radius $R\left(\theta\right)$ is given by

$$R\left(\theta\right) = C\ \left[1+\delta_2 Y_{20}\left(\theta\right)+\delta_4 Y_{40}\left(\theta\right)\right]. \qquad (30)$$

The angle θ is measured from the symmetry axis of the deformed nucleus.

We used the same density parameters as in the spherical Fermi shape, while the values of the deformation parameters (δ_2 and δ_4) were taken from Möller *et al.* [45]. The total α-core potential is given by

$$V(R,\beta) = V_N(R,\beta) + V_C(R,\beta) + \frac{\hbar^2(\ell+1/2)^2}{2\mu\ R^2}, \qquad (31)$$

where R is the distance between the mass centers of the α-particle and the deformed daughter nucleus, while β is the angle between the separation vector $\vec{R}$ and the symmetry axis of the daughter nucleus. The nuclear and Coulomb potentials are obtained from the double-folding model. For the spherical-deformed interacting pair, the double-folding potential is solved numerically by using the multipole expansion method as described in Refs. [46–49].

We now generalize our spherical calculations of the α-decay half-lives to the deformed case. The polar-angle-dependent penetration probability of α decay is given by

$$P_\beta = \exp\left[-2\int_{R_2(\beta)}^{R_3(\beta)}\sqrt{\frac{2\mu}{\hbar^2}\left|Q - V\left(R,\ \beta\right)\right|}\,dR\right], \qquad (32)$$

where $R_2(\beta)$ and $R_3(\beta)$ are the second and third classical turning points for a certain orientation angle β. The depth λ of the nuclear potential is renormalized for each orientation to ensure a quasistationary state by application of the Bohr-Sommerfeld quantization condition. Here the calculation of P_β in each direction is similar to the spherical calculation but the complexity and time of computation are much more than for the spherical calculation. The total penetration factor P is obtained by averaging P_β in all directions such that

$$P = \frac{1}{2}\int_0^\pi P_\beta \sin(\beta)\,d\beta. \qquad (33)$$

This averaging procedure is widely used in both α-decay and fusion reaction calculations [50–52]. The value of the assault frequency ν is also obtained by the same averaging procedure along different orientation angles. Finally, the α-decay width is given by

$$\Gamma = P_\alpha \hbar\nu\,\frac{1}{2}\int_0^\pi P_\beta \sin(\beta)d\beta. \qquad (34)$$

V. RESULTS AND DISCUSSION

α decay was the chosen mode of study because, in the case of the heaviest elements [1,2], α decay is the main decay mode, but for superheavies spontaneous fission competes. Another attractive feature that made α radioactivity the chosen mode of study is that α particles can be detected rather easily under favorable conditions such as high efficiency, low background, and good energy resolution. In even-even parent nuclei there is less uncertainty in the determination of the released energy Q value, which is one of the crucial factors for quantitative prediction of decay half-lives, and all the parent and daughter nuclei have zero spins and positive parities. Also, as a rule, in even-even nuclei, α transitions occur from ground state to ground state, which make their partial half-life systematics relatively smooth. Thus, the expectation is that the α-decay systematics of the chosen even-even nuclei would be good enough to provide a comprehensive study of shell closure in SHEs.

In the present work, we have calculated α-decay half-lives from ground state (g.s.) to ground state assuming zero angular momentum transfers (i.e, $\ell = 0$ transition) in even-even nuclei from Pb nucleus to superheavy nuclei. The Q value is a crucial quantity that strongly affects the calculation of the decay half-life, because the half-life is exponentially dependent on the Q value. In general, half-life calculations are very sensitive to Q values; in particular, α-decay half-lives, when calculated with experimental Q values, are found to be in better agreement with experimental half-lives. This was highlighted by Basu *et al.* in Ref. [36]. Therefore, we have adopted experimental Q values.

A. Behavior of α-decay half-lives near the neutron magic number $N = 126$

The aim of the present work was to test the possibility of extracting magic numbers for SHEs from the behavior of α-decay half-lives. First, we start with the well-known neutron magic number $N = 126$ and study the variation of α-decay half-lives as a function of nucleon number when N approaches 126 in the presence and absence of the proton magic number. In this regard, we considered Pb and Po isotope chains. We have calculated α-decay half-lives for different Pb isotopes, assuming a spherical shape, in the framework of the formulation described in Sec. IV. The input potential for the α + daughter system is obtained using the M3Y—Paris NN interaction of Eqs. (3) and (5). Implementation of the Bohr-Sommerfeld quantization condition, Eq. (20), fixes the strength of the nuclear potential λ in Eq. (12). The "fitted" global quantum number G appearing in Eq. (20) is taken to be 18. As discussed in Ref. [9], Xu *et al.* obtained a better set of parameters for the preformation factors $P_\alpha = 0.43$ for even-even nuclei, through a least-squares fit to the available experimental half-lives of the medium mass nuclei with proton number $Z = 52$–80. In this regard, two different values are used for the preformation probabilities $P_\alpha = 0.43$ and $P_\alpha = 1$. These values of the preformation factors lie in the experimental range $P_\alpha = 0.005$–1.0 [44].

The calculated α-decay half-lives together with the experimental Q values and the experimental half-lives for Pb isotopes [14,18] are presented in Table I. It is clearly demonstrated in Table I that there is a good agreement between our calculated results with $P_\alpha = 0.43$ and the corresponding experimental data on half-lives. Graphically, such good agreement is demonstrated in Fig. 1 in the cases of different isotopes of the Pb nucleus. Figure 1 and Table I indicate that the α-decay half-life of the Pb isotope increases by a factor of more than 10 with the addition of a pair of neutrons to the isotope ^{178}Pb. As the neutron magic number $N = 126$ is approached, the increase in α-decay half-life owing to the addition of a

TABLE I. Comparison between experimental α-decay half-lives [14,18] and results obtained with the M3Y—Paris effective interaction using $G = 18$ for Pb isotopes using two values of the preformation probabilities $P_\alpha = 1.00$ and 0.43.

Parent nucleus		M3Y—Paris, $T_{1/2}$ (ms)		Expt.	
Z	A	$P_\alpha = 1.00$	$P_\alpha = 0.43$	Q (MeV)	$T_{1/2}$ (ms)
82	178	0.13	0.30	7.790	0.23
82	180	1.76	4.10	7.415	5.00
82	184	249.16	579.45	6.774	610.00
82	186	3431.46	7980.13	6.470	12000.00
82	190	7.12×10^6	1.66×10^7	5.697	1.80×10^7
82	194	1.38×10^{12}	3.20×10^{12}	4.738	9.80×10^{12}

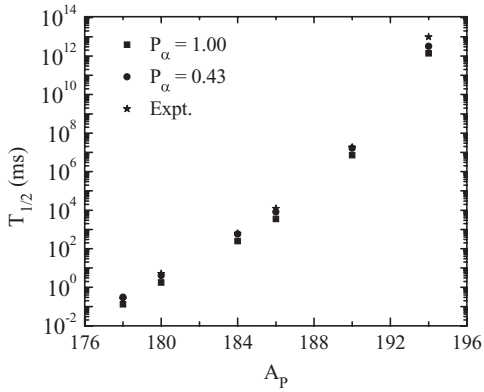

FIG. 1. α-decay half-lives for different isotopes of the Pb nucleus with mass number A_P. Half-lives are calculated in the framework of the double-folding model with M3Y—Paris using Eqs. (3) and (5) along with Eqs. (27) and (28) with global quantum number $G = 18$ for two values of preformation probability, $P_\alpha = 1.00$ and 0.43. Experimental Q values and half-lives were obtained from Refs. [14] and [18].

neutron pair to the parent nucleus becomes too large. For example, the α-decay half-life of ^{186}Pb is larger than that of ^{184}Pb by a factor of about 13, while the α-decay half-life of ^{194}Pb is larger than that of ^{184}Pb by a factor of about 5×10^9. This is mostly a Q-value effect and reflects the fact that the nucleus tends to be more stable as the proton and/or neutron numbers approach a magic number [53].

To study the correlation between the variation of the half-lives around the nucleon magic number and the nuclear shell effect, the half-lives of Po ($Z = 84$) isotopes are given as a function of the neutron number in Fig. 2. The experimental Q values and half-lives are obtained from Refs. [11,54,55]. It should be noted that the Po nucleus is different from the Pb nucleus in that the latter has proton magic number $Z = 82$, while the first nucleus has not. So, we expect different behavior of α-decay half-lives of Po isotopes compared to that of Pb isotopes.

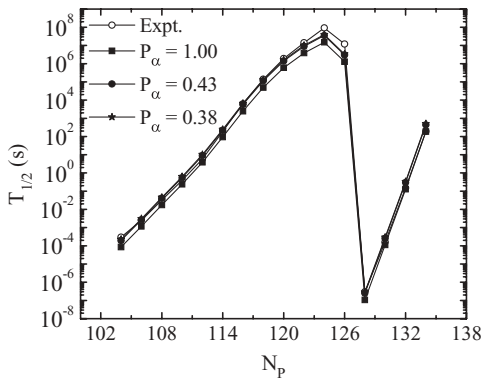

FIG. 2. The same as Fig. 1 but for different isotopes of the Po nucleus calculated using three values of preformation probability, $P_\alpha = 1.00, 0.43$, and 0.38. The global quantum number G is used as in Ref. [9] ($G = 18$ for $82 < N_P \leqslant 126$, while $G = 20$ for $N_P > 126$). Experimental Q values and half-lives are obtained from Refs. [11], [54], and [55].

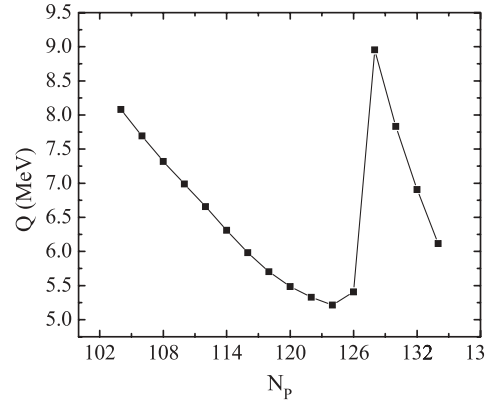

FIG. 3. Experimental released energies Q of α decay [54] for different isotopes of the Po nucleus with the neutron number N_P.

In Fig. 2 the change in half-lives with neutron number clearly shows that the shell effect plays an important role in α-decay half-lives. The closer the daughter nucleon number to the magic number, the greater the decrease in the half-life of the parent nucleus. Overall, the α-decay half-lives of the Po parent nucleus increases with increasing neutron number from $N_P = 104$ up to $N_P = 124$ and then decreases slightly at spherical shell closure $N_P = 126$. The addition of two neutrons to the magic number $N_P = 126$ of the Po parent nucleus produces too sharp decrease, by a factor more than 10^{13}, in its half-life for α emission. This is demonstrated in Table II upon comparing either the experimental or the theoretical α-decay half-lives for $A_p = 210$ and 212. This reflects the stability gained by the Po nucleus when N_P reaches the neutron magic number $N_P = 126$. On the contrary, the Po nucleus becomes unstable when the neutron number slightly exceeds the magic number.

One knows that the shell effect for α radioactivity is related to the Q value, which is maximum when the daughter nucleus has a magic number of neutrons and/or protons. According to Eqs. (21) and (22), shell effects are included in the penetration probability, which is related to the Q value. So the change in penetration probability is attributable to changes in Q. These features are clearly shown in Figs. 3 and 4.

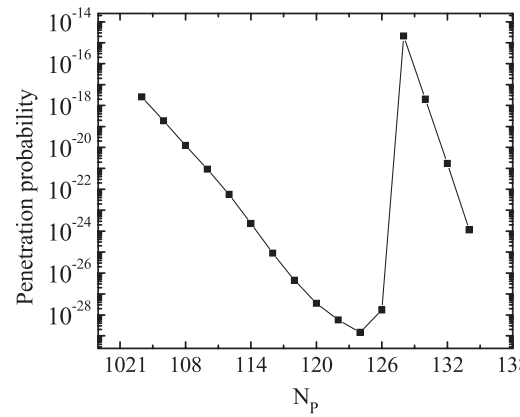

FIG. 4. Calculated penetration probability for different isotopes of the Po nucleus with the neutron number N_P.

TABLE II. The same as Table I but for different isotopes of the Po nucleus calculated using three values of preformation probability, $P_\alpha = 1.00$, 0.43, and 0.38. The global quantum number G is used as in Ref. [9] ($G = 18$ for $82 < N_P \leqslant 126$, while $G = 20$ for $N_P > 126$). Experimental Q values and half-lives were obtained from Refs. [11], [54], and [55].

Parent nucleus		M3Y—Paris, $T_{1/2}$ (s)			Expt.	
Z	A	$P_\alpha = 1.00$	$P_\alpha = 0.43$	$P_\alpha = 0.38$	Q (MeV)	$T_{1/2}$ (s)
84	188	8.47×10^{-5}	1.97×10^{-4}	2.23×10^{-4}	8.082	3×10^{-4}
84	190	1.16×10^{-3}	2.69×10^{-3}	3.05×10^{-3}	7.693	2.5×10^{-3}
84	192	1.75×10^{-2}	4.08×10^{-2}	4.61×10^{-2}	7.319	3.3×10^{-2}
84	194	2.37×10^{-1}	5.52×10^{-1}	6.24×10^{-1}	6.987	3.9×10^{-1}
84	196	3.85×10^{0}	8.96×10^{0}	1.01×10^{1}	6.657	5.9×10^{0}
84	198	0.93×10^{2}	2.17×10^{2}	2.46×10^{2}	6.309	1.9×10^{2}
84	200	2.47×10^{3}	5.74×10^{3}	6.49×10^{3}	5.981	6.2×10^{3}
84	202	4.87×10^{4}	1.13×10^{5}	1.28×10^{5}	5.701	1.4×10^{5}
84	204	6.04×10^{5}	1.41×10^{6}	1.59×10^{6}	5.485	1.9×10^{6}
84	206	3.82×10^{6}	8.89×10^{6}	1.01×10^{7}	5.327	1.4×10^{7}
84	208	1.49×10^{7}	3.47×10^{7}	3.93×10^{7}	5.215	9.1×10^{7}
84	210	1.28×10^{6}	2.99×10^{6}	3.38×10^{6}	5.407	1.2×10^{7}
84	212	1.08×10^{-7}	2.51×10^{-7}	2.83×10^{-7}	8.954	3.0×10^{-7}
84	214	1.11×10^{-4}	2.58×10^{-4}	2.92×10^{-4}	7.833	1.6×10^{-4}
84	216	1.27×10^{-1}	2.96×10^{-1}	3.35×10^{-1}	6.906	1.5×10^{-1}
84	218	1.88×10^{2}	4.38×10^{2}	4.95×10^{2}	6.115	1.9×10^{2}

TABLE III. The same as Table I but for Cm, Cf, Fm, and No isotope chains using the preformation probability $P_\alpha = 1.00$ with two possible fitted values of the global quantum number G, namely, 20 and 22. Moreover, α-decay half-lives are also calculated by including the deformation effect of the daughter nucleus, where the deformation parameters are taken from Möller *et al.* [45]. Experimental Q values and half-lives were obtained from Refs. [11], [54], and [55].

Parent nucleus		Spherical, $T_{1/2}$ (ms)		Deformed, $T_{1/2}$ (ms): $G = 20$	Expt.	
Z	A	$G = 20$	$G = 22$		Q (MeV)	$T_{1/2}$ (ms)
96	238	3.28×10^{8}	1.87×10^{8}	1.04×10^{8}	6.620	2.30×10^{8}
96	240	3.50×10^{9}	1.99×10^{9}	1.03×10^{9}	6.397	2.30×10^{9}
96	242	2.51×10^{10}	1.43×10^{10}	0.79×10^{10}	6.216	1.40×10^{10}
96	244	9.09×10^{11}	5.15×10^{11}	3.17×10^{11}	5.902	5.70×10^{11}
96	246	2.60×10^{14}	1.47×10^{14}	0.83×10^{14}	5.475	1.50×10^{14}
96	248	1.92×10^{16}	1.08×10^{16}	0.51×10^{16}	5.162	1.20×10^{16}
98	240	8.44×10^{4}	4.84×10^{4}	2.91×10^{4}	7.719	6.50×10^{4}
98	242	4.55×10^{5}	2.60×10^{5}	1.62×10^{5}	7.516	2.60×10^{5}
98	244	2.31×10^{6}	1.32×10^{6}	0.80×10^{6}	7.329	1.20×10^{6}
98	246	1.86×10^{8}	1.06×10^{8}	0.66×10^{8}	6.861	1.30×10^{8}
98	248	3.81×10^{10}	2.16×10^{10}	1.23×10^{10}	6.361	2.90×10^{10}
98	250	5.01×10^{11}	2.83×10^{11}	1.87×10^{11}	6.128	4.10×10^{11}
98	252	1.66×10^{11}	9.38×10^{10}	6.43×10^{10}	6.217	8.60×10^{10}
98	254	5.17×10^{12}	2.92×10^{12}	2.30×10^{12}	5.926	1.70×10^{12}
100	246	2.55×10^{3}	1.46×10^{3}	0.93×10^{3}	8.374	1.30×10^{3}
100	248	4.43×10^{4}	2.54×10^{4}	1.59×10^{4}	8.002	3.90×10^{4}
100	250	1.84×10^{6}	1.05×10^{6}	0.70×10^{6}	7.557	2.0×10^{6}
100	252	7.26×10^{7}	4.12×10^{7}	2.96×10^{7}	7.152	9.10×10^{7}
100	254	1.57×10^{7}	0.89×10^{7}	0.64×10^{7}	7.307	1.20×10^{7}
100	256	2.14×10^{8}	1.21×10^{8}	0.97×10^{8}	7.027	1.20×10^{8}
102	252	3.59×10^{3}	2.05×10^{3}	1.45×10^{3}	8.549	3.60×10^{3}
102	254	4.06×10^{4}	2.32×10^{4}	1.76×10^{4}	8.226	5.70×10^{4}
102	256	2.49×10^{3}	1.42×10^{3}	1.10×10^{3}	8.581	2.90×10^{3}

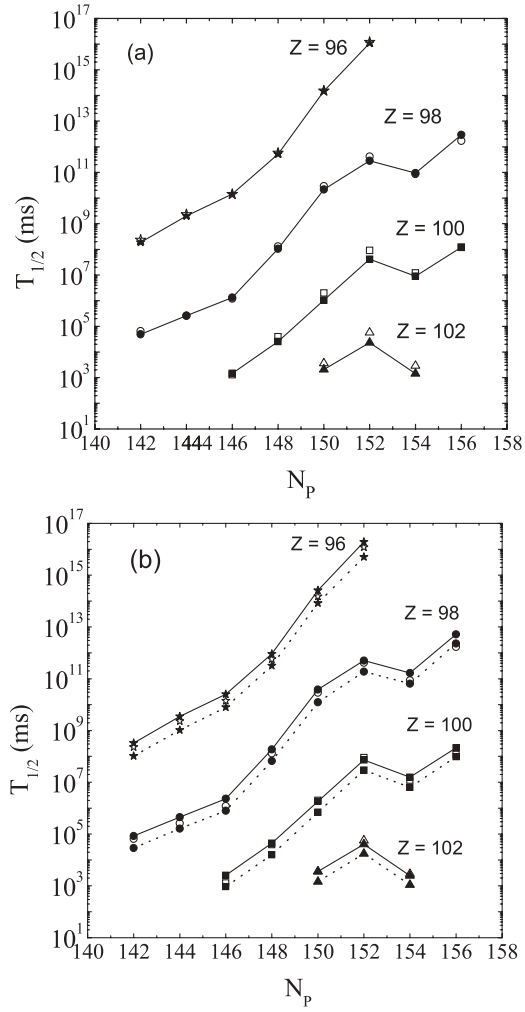

FIG. 5. α-decay half-lives for different isotopes of the ^{96}Cm, ^{98}Cf, ^{100}Fm, and ^{102}No nuclei with the neutron number N_P. Half-lives are calculated using the M3Y—Paris NN interaction assuming (a) *spherical* daughter nuclei with $G = 22$ (solid line with filled symbols) and (b) both *spherical* (solid line with filled symbols) and *deformed* (dotted lines with filled symbols) daughter nuclei with $G = 20$. Open symbols in (a) and (b) are for experimental half-lives [11,55].

B. Half-lives around the expected neutron submagic number $N = 152$

We calculate the α-decay half-lives of Cm, Cf, Fm, and No isotopes using their experimental released energies Q [54]. The agreement between the calculated α-decay half-lives, assuming spherical daughter nuclei, in the framework of the double-folding model with M3Y—Paris NN force using the preformation probability value $P_\alpha = 1$, and the experimental ones [55] are presented in Figs. 5(a) and 5(b). Two possible values of the "fitted" global quantum number G appearing in Eq. (21) are taken, $G = 20$ and 22. In Fig. 5(b), we further compare our predicted half-lives assuming spherical daughter nuclei with the deformed ones, as described in Sec. IV, for the previous isotopes using the same NN interaction, M3Y—Paris, with the global quantum number $G = 20$. The results of this calculation are also reported in Table III, together with both the spherical calculation and the experimental data for comparison. With such deformations, the calculated α-decay half-lives decrease by a factor of 2–3 compared to the spherical calculations. It is concluded that, owing to deformed barrier effects, the nuclear deformation mainly affects the barrier penetration probability of the α particle and hence decreases α-decay half-lives. Moreover, the general trends of α-decay half-lives with neutron number, shown in Fig. 5(b), are identical for both spherical and deformed calculations.

Figures 5(a) and 5(b) show that the α-decay half-lives increase as the value of Z decreases, which reflects the stability gained by these nuclei when two protons are removed. An obvious decrease that is not that prominent in the α-decay half-lives for Cf and Fm nuclei exists around the parent neutron number $N_P = 154$. We may conclude that $N = 152$ is a daughter-neutron submagic number. This is exactly the reason why this decrease is not as prominent. It should be noted that the effects of the deformed neutron shell at neutron number $N = 152$ have been experimentally observed for a long time [2,56,57]. Moreover, a deformed shell gap at $N = 152$ is predicted by the macroscopic-microscopic approach [58], and a recent experiment supported its existence at $Z = 100$ and $N = 152$ [59]. The results shown in Figs. 5(a) and 5(b) are reported in Table III. The table shows a good agreement between the calculated α-decay half-lives and the experimental data.

C. Half-lives around the expected neutron magic number $N = 162$

It is shown clearly in Figs. 1, 2, 5(a), and 5(b) that the calculated α-decay half lives are in quite good agreement with the experimental ones when the experimental Q values are used. In this regard, we can extrapolate our calculations to a region of nuclei where the experimental α-decay half-lives are unknown. The α-decay energies Q were obtained from Ref. [54]. The results for the calculated α-decay half-lives for different isotopes of the Sg, Hs, and 110 nuclei with neutron number N_P are shown in Fig. 6 with two different values of the global quantum number, $G = 20$ and 22. The calculated α-decay half-lives were compared with the estimated values by the well-known Viola-Seaborg semiempirical formula, which is given by

$$\log_{10} T_\alpha = (aZ + b)\, Q^{-1/2} + (cZ + d)\,, \qquad (35)$$

where the half-life T_α is in seconds, the Q value is in megaelectronvolts, and Z is the atomic number of the parent nucleus. Instead of using the original set of constants of Viola and Seaborg, we used more recent values that were proposed by Dong *et al.* [60] through a least-squares fit to even-even nuclei between $Z = 84$ and $Z = 110$, with $N > 126$.

Figure 6 shows that the α-decay half-lives with $G = 20$ are in close agreement with the Viola-Seaborg values for all isotopes. Moreover, the general trends of α-decay half-lives that can be seen when we approach a magic number are clearly shown in Fig. 6 around the parent neutron number $N_P = 164$. Thus, we may conclude that the daughter neutron number $N = 162$ is a magic number. Concerning the behavior of α-decay half-lives with the number of protons, Fig. 6 shows an increase in α-decay half lives by more than 10^3 when Z is reduced by

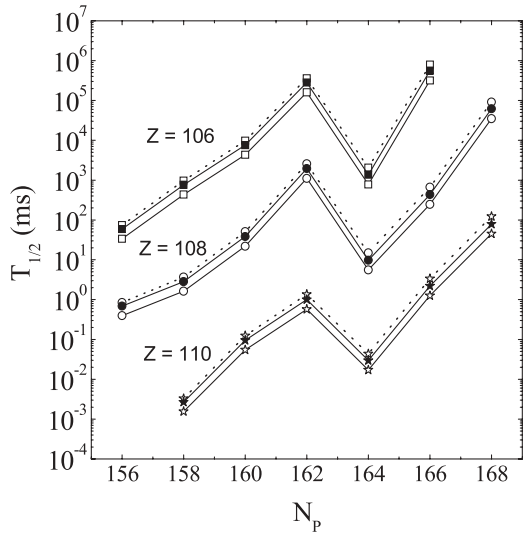

FIG. 6. α-decay half-lives for different isotopes of the ^{106}Sg, ^{108}Hs, and 110 nuclei with the neutron number N_P. Half-lives are calculated using the M3Y—Paris NN interaction assuming *spherical* daughter nuclei with $G = 20$ (solid line with filled symbols) and $G = 22$ (solid line with open symbols) and compared with the calculated half-lives from the Viola-Seaborg formula (dotted line with open symbols).

two protons at $Z = 110$ and $N_P = 162$. This factor is reduced to about 10^2 at $Z = 108$. Therefore the number of protons $Z = 108$ has more stability in our calculations.

D. Half-lives around the expected neutron magic number $N = 184$

We now extend the same method to isotopes of superheavy nuclei with $Z = 112$–120, where our results for the α-decay half-lives are compared with those estimated from the Viola-Seaborg formula in Fig. 7. We used the theoretical Q values extracted from the difference in mass excesses based on the

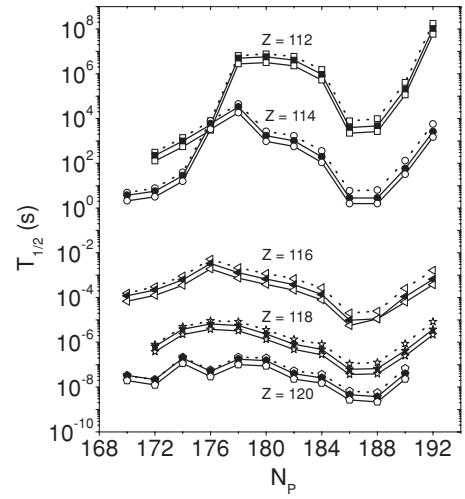

FIG. 7. The same as Fig. 6 but for superheavy nuclei with $Z = 112$, 114, 116, 118, and 120. Q values are extracted from the mass excesses, Eq. (36), based on the finite-range liquid drop model (FRLDM) of Ref. [45].

finite-range liquid drop model, FRLDM [45], as follows:

$$Q_{\rm th} = M - (M_\alpha + M_d) = \Delta M - (\Delta M_\alpha + \Delta M_d)\,, \qquad (36)$$

where M, M_α, M_d, ΔM, ΔM_α, and ΔM_d are the atomic masses and the atomic mass excesses of the parent nucleus, the emitted α particle, and the residual daughter nucleus, respectively, all expressed in units of energy.

The curves in Fig. 7 show an increase in the value of the α-decay half-lives for all studied superheavy isotopes at the parent neutron number $N_P = 188$. A relatively strong decrease occurs at $N_P = 184$ and the values of the α-decay half-lives are almost the same at $N_P = 186$ and 188. It should be noted that the existence of enhanced stability at $N = 184$ is consistent with the suggested magic numbers in the relativistic continuum Hartree-Bogoliubov theory (RCHB) for all effective interactions used in Ref. [61]. The predicted proton magic number $Z = 114$ is clear in Fig. 7 from the large

TABLE IV. Comparison between experimental α-decay half-lives [62–64] and results obtained with M3Y—Paris, M3Y—Reid, DDM3Y1, and DDM3Y2 effective interactions using $G = 22$ for superheavy elements.

Parent nucleus		$T_{1/2}$				Expt.	
Z	A	M3Y—Paris	M3Y—Reid	DDM3Y1	DDM3Y2	Q (MeV)	$T_{1/2}$
118	294	0.42 ms	0.41 ms	0.09 ms	0.06 ms	11.81 ± 0.06	$0.89^{+1.07}_{-0.31}$ ms
116	292	27.53 ms	26.93 ms	5.92 ms	4.08 ms	10.80 ± 0.07	18^{+16}_{-6} ms
116	290	9.06 ms	8.86 ms	1.95 ms	1.35 ms	11.00 ± 0.08	$7.1^{+3.2}_{-1.7}$ ms
114	288	0.51 s	0.50 s	0.11 s	0.08 s	10.09 ± 0.07	$0.8^{+0.32}_{-0.18}$ s
114	286	0.10 s	0.10 s	0.02 s	0.016 s	10.35 ± 0.06	$0.16^{+0.07}_{-0.03}$ s
112	284	16.68 s	16.31 s	3.58 s	2.47 s	9.35 ± 0.05	$9.8^{+18}_{-3.8}$ s
110	270	43.99 μs	43.09 μs	9.87 μs	7.07 μs	11.24 ± 0.05	100^{+140}_{-40} μs
108	266	1.25 ms	1.22 ms	0.28 ms	0.20 ms	10.38 ± 0.02	$2.3^{+1.3}_{-0.6}$ ms
108	264	0.40 ms	0.39 ms	0.09 ms	0.06 ms	10.59 ± 0.05	0.54 ± 0.3 ms
106	266	5.96 s	5.83 s	1.31 s	0.93 s	8.84 ± 0.02	$25.7 \pm X$ s

TABLE V. The same as Table IV but with $G = 20$.

Parent nucleus		$T_{1/2}$				Expt.	
Z	A	M3Y—Paris	M3Y—Reid	DDM3Y1	DDM3Y2	Q (MeV)	$T_{1/2}$
118	294	0.74 ms	0.73 ms	0.16 ms	0.11 ms	11.81 ± 0.06	$0.89^{+1.07}_{-0.31}$ ms
116	292	48.70 ms	47.54 ms	10.61 ms	7.13 ms	10.80 ± 0.07	18^{+16}_{-6} ms
116	290	16.00 ms	15.62 ms	3.49 ms	2.35 ms	11.00 ± 0.08	$7.1^{+3.2}_{-1.7}$ ms
114	288	0.90 s	0.88 s	0.20 s	0.13 s	10.09 ± 0.07	$0.8^{+0.32}_{-0.18}$ s
114	286	0.18 s	0.18 s	0.04 s	0.03 s	10.35 ± 0.06	$0.16^{+0.07}_{-0.03}$ s
112	284	29.64 s	28.94 s	6.45 s	4.34 s	9.35 ± 0.05	$9.8^{+18}_{-3.8}$ s
110	270	76.37 μs	74.66 μs	17.32 μs	12.09 μs	11.24 ± 0.05	100^{+140}_{-40} μs
108	266	2.18 ms	2.13 ms	0.49 ms	0.34 ms	10.38 ± 0.02	$2.3^{+1.3}_{-0.6}$ ms
108	264	0.69 ms	0.68 ms	0.16 ms	0.11 ms	10.59 ± 0.05	0.54 ± 0.3 ms
106	266	10.49 s	10.25 s	2.34 s	1.61 s	8.84 ± 0.02	$25.7 \pm X$ s

increase in the α-decay half-lives by reducing $Z = 116$ by two protons. In this case the value of the α-decay half-life increases by a factor of 1.4×10^6 at $N_P = 184$, reflecting great stability of the parent nucleus at $Z = 114$.

E. Sensitivity of superheavy half-lives to the nucleon-nucleon force

Most recent calculations of α-decay half-lives use M3Y—Reid or its density-dependent version, DDM3Y, given by Eq. (9). The calculations are usually performed in the WKB framework using two different approaches. The first approach, the super asymmetric fission model [35,36,40,41], is based on multiplying the NN force by a normalization factor determined from the best fit to the experimental α-decay half-lives. The second approach, the density-dependent cluster model [8,9], determines the normalization factor λ in the nuclear potential, Eqs. (12) and (18), by applying the Bohr-Sommerfeld quantization condition [22]. In the present study, we used the second approach and derived the α-nucleus potential using four types of M3Y NN force.

In Tables IV and V, the α-decay half-lives of some known superheavy nuclei [62–64] are shown for two choices of the global quantum number G of the Bohr-Sommerfeld quantization condition. The results obtained using Eqs. (3) and (5) for the free NN interaction are labeled M3Y—Paris in Tables IV and V, while M3Y—Reid represents the results obtained using Eqs. (2) and (4). The density-dependent NN interaction, DDM3Y1, calculations use Eqs. (2), (4), and (6)–(8) in Eq. (18), while calculations performed with density-dependent NN interaction, DDM3Y2, make use of a power-law dependence on ρ through Eqs. (2), (4), and (9) in Eq. (18).

One can see that the introduction of density dependence in the NN interaction in the density-dependent cluster model reduces the lifetimes by about an order of magnitude compared to the free NN results. Also, comparing the α-decay half-lives for some nuclei, listed in Tables IV and V and the corresponding quantities calculated for the same nuclei in Ref. [36] using the DDM3Y2 force within the super asymmetric fission model, one concludes that the Bohr-Sommerfeld condition, when applied to density-dependent NN interactions, reduces the α-decay half-lives by about an order of magnitude [22]. Moreover, a good agreement exists between the calculations of the α-decay half-lives with the free NN force as in M3Y—Reid or M3Y—Paris and the experimental half-lives of the superheavy nuclei listed in Tables IV and V. The free NN force M3Y—Paris slightly enhances the α-decay half-lives compared to the Reid version. The exponential form of the density dependence, DDM3Y1, increases the α-decay half-lives by a factor of about 1.5 compared to the DDM3Y2 NN force. Comparing the results of α-decay half-lives in Tables IV and V, one observes that the half-lives are reduced when the value of the global quantum number is increased from $G = 20$ to $G = 22$. It should be pointed out that the change in the global quantum number can be used to compensate for a density-dependent interaction.

VI. SUMMARY AND CONCLUSION

Nuclear potentials have been calculated by the double-folding model with an M3Y—Paris NN interaction with the matter density distributions of a daughter nucleus and an α particle. The Coulomb potential is also obtained from the double-folding technique to be consistent with the microscopic nuclear potential. In the framework of the WKB approximation, α-decay half-lives of heavy elements and SHEs are calculated and compared with the experimental data. The obtained α-decay half-lives agree reasonably well with the available experimental data. Deformation of the daughter nucleus reduces the calculated α-decay half-lives by a factor of 2–3, compared to the spherical shape, and does not affect the behavior of α-decay half-lives with neutron number.

The change in α-decay half-lives with neutron number shows that shell effects play an important role in *the behavior of* α-decay half-lives around magic numbers. The closer the daughter nucleon number to the magic number, the greater the decrease in the half-lives of the parent nuclei. The α-decay calculations give the closed-shell effects of known spherical magicities, $Z = 82$ and $N = 126$, and further predict enhanced

stabilities at $N = 152$, 162, and 184, with $Z = 100$, 108, and 114, owing to the stability of parents nuclei against α decays.

Moreover, the study has been extended to the newly observed superheavy nuclei. The α-decay half-lives of superheavy nuclei are sensitive to the input of density dependence in the NN interaction of nucleons in the α particle and the daughter nucleus, as the half-lives can decrease by an order of magnitude compared to the results with a free NN interaction.

[1] S. Hofmann, Rep. Prog. Phys. **61**, 639 (1998).
[2] S. Hofmann and G. Münzenberg, Rev. Mod. Phys. **72**, 733 (2000).
[3] J. O. Rasmussen, in *Alpha-, Beta-, and Gamma-Ray Spectroscopy*, edited by K. Siegbahn (North Holland, Amsterdam, 1965), Vol. I, p. 701.
[4] Yu. Ts. Oganessian *et al.*, Nature (London) **400**, 242 (1999).
[5] G. Gamow, Z. Phys. **51**, 204 (1928).
[6] E. U. Condon and R. W. Gurney, Nature **122**, 439 (1928).
[7] B. Buck, A. C. Merchant, and S. M. Perez, At. Data Nucl. Data Tables **54**, 53 (1993).
[8] C. Xu and Z. Ren, Phys. Rev. C **74**, 014304 (2006); **73**, 041301(R) (2006).
[9] C. Xu and Z. Ren, Nucl. Phys. **A760**, 303 (2005); **A753**, 174 (2005).
[10] P. Mohr, Phys. Rev. C **61**, 045802 (2000).
[11] J. C. Pei, F. R. Xu, Z. J. Lin, and E. G. Zhao, Phys. Rev. C **76**, 044326 (2007).
[12] V. Y. Denisov and H. Ikezoe, Phys. Rev. C **72**, 064613 (2005).
[13] G. Royer, J. Phys. G **26**, 1149 (2000).
[14] G. Royer and H. F. Zhang, Phys. Rev. C **77**, 037602 (2008).
[15] H. F. Zhang and G. Royer, Phys. Rev. C **76**, 047304 (2007).
[16] D. S. Delion, R. J. Liotta, and R. Wyss, Phys. Rev. C **76**, 044301 (2007).
[17] P. Mohr, Phys. Rev. C **73**, 031301(R) (2006).
[18] B. Sahu, Phys. Rev. C **78**, 044608 (2008).
[19] G. Wentzel, Z. Phys. **38**, 518 (1926); H. A. Kramers, *ibid.* **39**, 828 (1923); see also the reference list in, L. Schiff, *Quantum Mechanics*, 3rd ed. (McGraw-Hill, New York, 1968).
[20] G. Drukarev, N. Fröman, and P. O. Fröman, J. Phys. A **12**, 171 (1979).
[21] R. G. Lovas, R. J. Liotta, A. Insolia, K. Varga, and D. S. Delion, Phys. Rep. **294**, 265 (1998).
[22] N. G. Kelkar and H. M. Castañeda, Phys. Rev. C **76**, 064605 (2007).
[23] I. Tonozuka and A. Arima, Nucl. Phys. **A323**, 45 (1979).
[24] H. Horiuchi, Nucl. Phys. **A522**, 257 (1991).
[25] H. Takemoto, M. Fukushima, S. Chiba, H. Horiuchi, Y. Akaishi, and A. Tohsaki, Phys. Rev. C **69**, 035802 (2004).
[26] G. Bertsch, J. Borysowicz, H. McManus, and W. G. Love, Nucl. Phys. **A284**, 399 (2004).
[27] G. R. Satchler and W. G. Love, Phys. Rep. **55**, 183 (1979).
[28] C. Samanta, Y. Sakuragi, M. Ito, and M. Fujiwara, J. Phys. G **23**, 1697 (1997).
[29] A. M. Kobos, B. A. Brown, R. Lindsay, and G. R. Satchler, Nucl. Phys. **A425**, 205 (1984).
[30] W. von Oertzen, D. T. Khoa, and H. G. Bohlen, Europhys. News **31**, 5 (2000).
[31] M. E. Brandan and G. R. Satchler, Phys. Rep. **285**, 143 (1997).
[32] D. T. Khoa and W. von Oerzen, Phys. Lett. **B304**, 8 (1993).
[33] A. M. Kobos, B. A. Brown, P. E. Hodgson, G. R. Satchler, and A. Budzanowski, Nucl. Phys. **A384**, 65 (1982).
[34] M. El-Azab Farid and G. R. Satchler, Nucl. Phys. **A438**, 525 (1985).
[35] P. R. Chowdhury, C. Samanta, and D. N. Basu, At. Data Nucl. Data Tables **94**, 781 (2004).
[36] P. R. Chowdhury, C. Samanta, and D. N. Basu, Phys. Rev. C **73**, 014612 (2004).
[37] R. E. Langer, Phys. Rev. **51**, 669 (1937).
[38] J. J. Morehead, J. Math. Phys. **36**, 5431 (1995).
[39] J. D. Walecka, *Theoretical Nuclear Physics and Subnuclear Physics* (Oxford University Press, Oxford, 1995), pp. 11–13.
[40] C. Samanta, P. R. Chowdhury, and D. N. Basu, Nucl. Phys. **A789**, 142 (2007).
[41] P. R. Chowdhury, D. N. Basu, and C. Samanta, Phys. Rev. C **75**, 047306 (2007).
[42] B. Buck, A. C. Merchant, and S. M. Perez, Phys. Rev. C **45**, 2247 (1992); B. Buck, J. C. Johnston, A. C. Merchant, and S. M. Perez, *ibid.* **53**, 2841 (1996).
[43] S. A. Gurvitz and G. Kälbermann, Phys. Rev. Lett. **59**, 262 (1987).
[44] P. E. Hodgeson and E. Betak, Phys. Rep. **374**, 1 (2003).
[45] P. Möller, J. R. Nix, W. D. Myers, and W. J. Świtecki, At. Data Nucl. Data Tables **59**, 185 (1995).
[46] M. J. Rhoades-Brown, V. E. Oberacker, M. Seiwert, and W. Greiner, Z. Phys. A **310**, 287 (1983).
[47] M. Ismail, A. Y. Ellithi, and F. Salah, Phys. Rev. C **66**, 017601 (2002).
[48] M. Ismail, W. M. Seif, and H. El-Gebaly, Phys. Lett. **B563**, 53 (2003).
[49] M. Ismail, W. M. Seif, A. Y. Ellithi, and F. Salah, J. Phys. G **35**, 075101 (2008).
[50] Y.-J. Shi and W. J. Swiatecki, Nucl. Phys. **A464**, 205 (1987).
[51] T. L. Stewart, M. W. Kermode, D. J. Beachey, N. Rowley, I. S. Grant, and A. T. Kruppa, Nucl. Phys. **A611**, 332 (1996).
[52] V. Yu. Denisov and H. Ikezoe, Phys. Rev. C **72**, 064613 (2005).
[53] G. L. Zhang, X. Y. Lea, and H. Q. Zhang, Nucl. Phys. **A823**, 16 (2009).
[54] G. Audi, A. H. Wapstra, and C. Thibault, Nucl. Phys. **A729**, 337 (2003).
[55] G. Audi, O. Bersillon, J. Blachot, and A. H. Wapstra, Nucl. Phys. **A729**, 3 (2003).
[56] E. R. Flynn, G. L. Struble, R. G. Lanier, and L. G. Mann, Phys. Lett. **B67**, 158 (1977).
[57] A. Sobiczewski, Acta Phys. Pol. B **28**, 21 (1997).
[58] S. Ćwiok, S. Hofmann, and W. Nazarewicz, Nucl. Phys. **A573**, 356 (1994).
[59] P. T. Greenlees, Phys. Rev. C **78**, 021303(R) (2008).
[60] T. Dong and Z. Ren, Eur. Phys. J. A **26**, 69 (2004).
[61] W. Zhang, J. Meng, S. Q. Zhang, L. S. Geng, and H. Toki, Nucl. Phys. **A753**, 106 (2005).
[62] Yu. Ts. Oganessian *et al.*, Phys. Rev. C **74**, 044602 (2006); see references therein.
[63] Yu. Ts. Oganessian *et al.*, Phys. Rev. C **70**, 064609 (2004); **71**, 029902 (2004).
[64] Yu. Ts. Oganessian, Nucl. Phys. **A787**, 343 (2007).